

# Flavour structure of low-energy hadron pair photoproduction

K. Odagiri<sup>1</sup> and R.C. Verma<sup>2,a</sup>

<sup>1</sup> Institute of Physics, Academia Sinica, Nankang, Taipei, Taiwan 11529, The Republic of China

<sup>2</sup> Physics Division, National Center for Theoretical Sciences, Hsinchu, Taiwan 300, The Republic of China

November 8, 2018

**Abstract.** We consider the process  $\gamma\gamma \rightarrow H_1\bar{H}_2$  where  $H_1$  and  $H_2$  are either mesons or baryons. The experimental findings for such quantities as the  $p\bar{p}$  and  $K_S K_S$  differential cross sections, in the energy range currently probed, are found often to be in disparity with the scaling behaviour expected from hard constituent scattering. We discuss the long-distance pole–resonance contribution in understanding the origin of these phenomena, as well as the amplitude relations governing the short-distance contribution which we model as a scaling contribution. When considering the latter, we argue that the difference found for the  $K_S K_S$  and the  $K^+ K^-$  integrated cross sections can be attributed to the  $s$ -channel isovector component. This corresponds to the  $\rho\omega \rightarrow a$  subprocess in the VMD (vector-meson-dominance) language. The ratio of the two cross sections is enhanced by the suppression of the  $\phi$  component, and is hence constrained. We give similar constraints to a number of other hadron pair production channels. After writing down the scaling and pole–resonance contributions accordingly, the direct summation of the two contributions is found to reproduce some salient features of the  $p\bar{p}$  and  $K^+ K^-$  data.

**PACS.** 11.30.Hv Flavour symmetries – 12.40.-y Other models for strong interactions – 12.40.Nn Regge theory, duality, absorptive/optical models – 12.40.Vv Vector-meson dominance – 13.66.Bc Hadron production in  $e^-e^+$  interactions

## 1 Introduction

We consider the exclusive pair production process  $\gamma\gamma \rightarrow H_1\bar{H}_2$  where  $H_1$  and  $H_2$  are either mesons or baryons. We consider the energy region not too far from the threshold, for example the centre-of-mass energy  $W_{\gamma\gamma} < 4$  GeV.

It has been found that some of the results of recent large-statistics measurement of these processes, for example at Belle [1,2], are difficult to reconcile with theoretical thinking based on hard constituent scattering. For example, there is a violation of the scaling behaviour expected from the naive quark-counting rule [3],

$$\frac{d\sigma}{dt} \propto \frac{\cos\theta^*}{s^{K-2}}, \quad (1)$$

where  $K$  is the number of ‘elementary’ fields taking part in the interaction. For instance,  $K = 1 + 1 + 2 + 2 = 6$  for  $\gamma\gamma \rightarrow \pi\pi$ .  $s$  and  $t$  are the usual Mandelstam variables. After integration over a constant  $\cos\theta^*$  interval where  $\theta^*$  is the polar angle of scattering in the centre-of-mass frame, this yields:

$$\sigma \propto 1/s^3 \text{ (mesons)}, \quad 1/s^5 \text{ (baryons)}. \quad (2)$$

This scaling is expected to hold when the constituent-level hard subprocess approximately has a tree-level perturbative description. As seen in fig. 1, this fails for  $\gamma\gamma \rightarrow p\bar{p}$  [1,4,5,6] in the measured energy range. It seems to work for  $\gamma\gamma \rightarrow K^+ K^-$  [2,7,8] above  $W_{\gamma\gamma} \approx 2.4$  GeV but, disturbingly, seems to fail for  $\gamma\gamma \rightarrow K_S K_S$  [9] in the measured energy range of up to  $W_{\gamma\gamma} \approx 4$  GeV. The latter cross section drops faster with  $W_{\gamma\gamma}$ , and this finding, together with the large ratio between the two cross sections, is difficult to explain in frameworks based on hard constituent scattering. On the other hand, in the large-energy limit of the measured range, it has been found that the calculations of ref. [10], based on leading-term QCD and wave functions following from the QCD sum rules, can accommodate the value found experimentally.

Our main region of interest in this paper is below this energy range, where perturbative description is insufficient to account for the prominent features of the data. We are interested in the participation of alternative dynamics, that are more long-distance in nature, and are more appropriate to describing the observed distributions. At the same time, we are also interested in modelling the short-distance contribution with constraints from the amplitude factorization considerations.

As a starting-point, let us consider VMD (vector-meson dominance). Here, the photon is interpreted as a quark-antiquark object, so that the exponent  $K$  in eqn. (1) is

<sup>a</sup> Permanent address: Department of Physics, Punjabi University, Patiala-147002, India

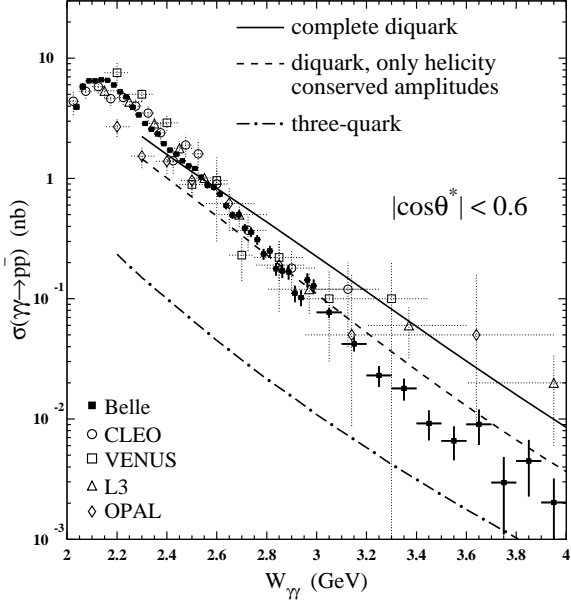


**Fig. 1.**  $\gamma\gamma \rightarrow p\bar{p}$  cross section [1] versus centre-of-mass energy at VENUS [4], CLEO [5] and Belle [1] in the central region, defined by  $|\cos\theta^*| < 0.6$ . The vertical error-bars on the Belle data are due to the statistical error in the event and the Monte Carlo samples only. Experimental data is compared against three theoretical calculations, as described in ref. [1]. Figure reproduced with kind permission of the authors of ref. [1].

modified. Corresponding to eqn. (2), we would have:

$$\sigma \propto 1/s^5 \text{ (mesons)}, \quad 1/s^7 \text{ (baryons)}. \quad (3)$$

Although the applicability of the quark-counting rule to the VMD picture should not be taken for granted, this indicates that the fall in the cross section with the centre-of-mass energy would be more rapid than is expected from eqn. (1). It is a curious finding that for central events, defined by  $|\cos\theta^*| < 0.6$ , the cross sections measured at Belle for  $\gamma\gamma \rightarrow K_S K_S$  [9] and  $p\bar{p}$  [1] go as  $\sim W_{\gamma\gamma}^{-(8\sim 12)}$  and  $\sim W_{\gamma\gamma}^{-(12\sim 15)}$  respectively for some regions of  $W_{\gamma\gamma}$  away from the resonance region. As the exponent is sensitive to the cut on  $|\cos\theta^*|$ , it is possible that this agreement with eqn. (3) is accidental. We note nevertheless that a result of the form above can be derived from the consideration of the Sudakov form-factor effects [11,12].

Encouraged by this finding, we go on to consider the factorization of the scattering amplitude into the production and decay parts. The production subprocess is dominated, in case of ideal mixing between  $\omega$  and  $\phi$ , by:

$$\rho^0 \rho^0, \omega\omega \rightarrow f_{ud}, \quad (4)$$

$$\rho^0 \omega, \omega \rho^0 \rightarrow a, \quad (5)$$

$$\phi\phi \rightarrow f_s. \quad (6)$$

In the above,  $f_{ud}$  stands for the  $(u\bar{u} + d\bar{d})/\sqrt{2}$  state. After relaxing the condition of ideal mixing,  $f_{ud}$  and  $f_s$  mix to

give the physical  $f$  and  $f'$  mesons. We are not necessarily adopting the  $s$ -channel resonance picture, and  $f$  and  $a$  are, for now, merely a label of the  $s$ -channel flavour structure.

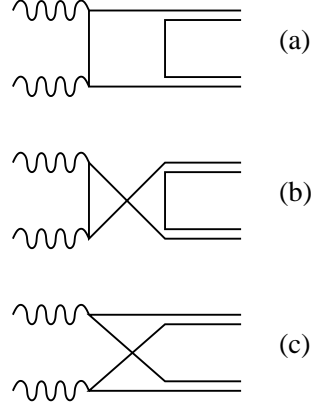


**Fig. 2.** The quark-line diagrams for meson-pair production. Similar diagrams can be drawn for the baryon-pair case. Diagrams (a) and (b) have  $s$ -channel representation whereas the 4-quark mode (c) does not.

The quark-line diagrams are shown in fig. 2. The production-decay factorization assumption implicitly corresponds to the choice of ‘handbag’ diagrams (a) and (b) of fig. 2, neglecting the 4-quark intermediate state of ‘cat’s-ears’ diagram (c). When considering long-distance dynamics, due to the degeneracy of the meson trajectories, we shall argue later that this approximation is acceptable for meson-pair production but not for baryon-pair production. On the other hand, while calculating the short-distance contribution, the relative size of the cat’s-ears diagram is sensitive to the factorization scheme adopted. Here we limit ourselves to remarking that in the findings of ref. [13], and for the energy range currently probed by experiment, their so-named ‘handbag’ approach is appropriate for describing some features of the data at hand. For instance, the angular distribution for the  $K_S K_S$  process, as seen in ref. [9], is in better agreement than the more traditional approach of ref. [10], although the overall normalization is not well understood in either of the two approaches.

We have also neglected the OZI-suppressed channels such as  $\rho^0 \phi \rightarrow f$ . The decay part can be expressed similarly.

We see immediately that any difference between the  $K^+ K^-$  and  $K^0 \bar{K}^0 = K_L K_L + K_S K_S$  cross sections must be due to the simultaneous presence of the isoscalar  $f/f'$  and isovector  $a = (u\bar{u} - d\bar{d})/\sqrt{2}$  components. It is also not difficult to see that the large ratio between  $K^+ K^-$  and  $K_S K_S$  processes can be increased by the suppression of  $\phi\phi \rightarrow f_s$ .

We proceed by modelling the short-distance piece as a scaling contribution obeying eqns. (1,2). The long-distance piece includes the resonances of eqns. (4)–(6). These are related to the  $t$ -channel pole picture by duality, so that we can also model them as Regge amplitudes [14,15]. The

signature term in the latter case would then represent the ‘cat’s-ears’ contributions.

We find that the direct summation of the two amplitudes reproduces some of the salient features of the  $K^+K^-$  and  $p\bar{p}$  data, although the description of the angular distribution in the former case is poor.

The modelling of the full amplitude as the sum of the two contributions at first sight may seem to suffer from the problem of double counting. However, we find numerically that adopting the alternative approach of a form factor that interpolates between the two amplitude in general cannot yield these results. An intuitive explanation would be that the finite-time short-distance effects and infinite-time Regge-pole dynamics have little overlap. More explicitly, short-distance amplitudes involve a finite and small number of intermediate particles that individually carry large virtuality, and are independent from the long-distance amplitudes where virtuality is assigned, in the parton language, collectively to the intermediate state partons. Hence in our understanding, any discrepancy with the data that arise are due to our ignorance of low-energy dynamics, rather than being due to some form of double-counting in this summation procedure. In any case, such approach is not new. For a well-known example involving the summation of short-distance and long-distance amplitudes, see ref. [16].

This paper is organized as follows. In sec. 2, we present the relevant Clebsch-Gordan coefficients for kaons and for other mesons and baryons. In sec. 3, we consider the effect of pole(-resonance) dynamics. The conclusions are stated at the end.

## 2 $SU(3)$ analysis

We decompose the  $(2 \rightarrow 2)$  amplitudes into the  $s$ -channel production part and the decay part, so that, for example, the  $s$ -channel scalar part of the amplitudes is given by:

$$\begin{aligned} \mathcal{A}(\gamma\gamma \rightarrow V_1 V_2 \rightarrow S \rightarrow H_1 \bar{H}_2) \\ = \gamma_{V_1}^{-1} \gamma_{V_2}^{-1} g_{V_1 V_2 S} \times g_{S H_1 H_2} \times F(S). \end{aligned} \quad (7)$$

$g$  are proportional to the  $SU(3)$  flavour Clebsch-Gordan coefficients, whereas the dynamics is contained in the function  $F(S)$ .  $\gamma_V$  are the photon- $V$  coupling constants satisfying:

$$\gamma_{\rho^0}^{-1} : \gamma_{\omega}^{-1} : \gamma_{\phi}^{-1} \approx 3 : 1 : -\sqrt{2}. \quad (8)$$

We shall adopt the ratio  $3 : 1$  for the  $\rho^0$  and  $\omega$  couplings later on, but modify the  $\phi$  coupling by a suppression factor  $\sqrt{\delta}$ . It should be understood that this suppression factor is introduced in order to suppress  $f'$  contribution. The photon coupling to  $\phi$  is not changed.

We note that the  $p\bar{p}$  data [1] shows clear indication of the presence of a pseudoscalar  $\eta_c$  resonance, and the same peak is also present in the  $K\bar{K}$  data [2]. The pseudoscalar contribution can be included without modifying the structure of the formalism.

## 2.1 Production subprocess

$u, d$  and  $s$  quarks are organized into a flavour triplet structure as:

$$\mathbf{3} \equiv q_a \equiv \begin{pmatrix} u \\ d \\ s \end{pmatrix}, \quad \mathbf{3}^* \equiv \bar{q}^a \equiv (\bar{u} \ \bar{d} \ \bar{s}). \quad (9)$$

Mesons are in  $\mathbf{3} \otimes \mathbf{3}^*$  and baryons are in  $\mathbf{3} \otimes \mathbf{3} \otimes \mathbf{3}$ .

We define the nonet  $1^-, 0^-,$  and  $0^+$  mesons by  $V_b^a, P_b^a,$  and  $S_b^a$ , respectively. These are constructed explicitly as:

$$\mathbf{3} \otimes \mathbf{3}^* \equiv \begin{pmatrix} u\bar{u} & u\bar{d} & u\bar{s} \\ d\bar{u} & d\bar{d} & d\bar{s} \\ s\bar{u} & s\bar{d} & s\bar{s} \end{pmatrix}, \quad (10)$$

$$V_b^a = \begin{pmatrix} \frac{\rho^0 + \omega \cos \theta_V - \phi \sin \theta_V}{\sqrt{2}} & \rho^+ & K^{*+} \\ \rho^- & \frac{-\rho^0 + \omega \cos \theta_V - \phi \sin \theta_V}{\sqrt{2}} & K^{*0} \\ K^{*-} & \frac{\sqrt{2}}{K^{*0}} & \omega \sin \theta_V + \phi \cos \theta_V \end{pmatrix} \quad (11)$$

$$P_b^a = \begin{pmatrix} \frac{1}{\sqrt{2}}\pi^0 + \frac{1}{\sqrt{6}}\eta_8 + \frac{1}{\sqrt{3}}\eta_1 & \pi^+ & K^+ \\ \pi^- & -\frac{1}{\sqrt{2}}\pi^0 + \frac{1}{\sqrt{6}}\eta_8 + \frac{1}{\sqrt{3}}\eta_1 & K^0 \\ K^- & \frac{K^0}{\sqrt{6}} & -\frac{2}{\sqrt{6}}\eta_8 + \frac{1}{\sqrt{3}}\eta_1 \end{pmatrix} \quad (12)$$

$$S_b^a = \begin{pmatrix} u\bar{u} & a_0^+ & K_0^+ \\ a_0^- & d\bar{d} & K_0^0 \\ K_0^- & \bar{K}_0^0 & s\bar{s} \end{pmatrix}. \quad (13)$$

We have defined the  $\omega - \phi$  mixing angle  $\theta_V$  in the above. For ideal mixing,  $\theta_V = 0$ .

The Clebsch-Gordan coefficients for the production subprocesses of eqns. (4)–(6) are calculated by the contribution of the diagonal,  $a = b = c$ , part of the quantity:

$$\frac{1}{2} (V_b^c V_c^a + V_c^a V_b^c) S_a^b. \quad (14)$$

This particular notation implies spin-0 state in the  $s$ -channel, but the structure of the expression is general to any even-spin positive parity states. The  $f - f'$  mixing angle  $\theta_S$  is defined by:

$$a_0 = (u\bar{u} - d\bar{d})/\sqrt{2}, \quad (15)$$

$$f_0 = \cos \theta_S (u\bar{u} + d\bar{d})/\sqrt{2} + \sin \theta_S (s\bar{s}), \quad (16)$$

$$f'_0 = -\sin \theta_S (u\bar{u} + d\bar{d})/\sqrt{2} + \cos \theta_S (s\bar{s}). \quad (17)$$

For later use, we define  $\theta_P$  analogously, which describes  $\eta - \eta'$  mixing.

The Clebsch-Gordan coefficients can now be calculated, and these are listed in tab. 1. We show the general case as well as the two cases of ideal mixing, corresponding to  $\theta_V = 0$  and to  $\theta_V = \theta_S = 0$ . In reality,  $\theta_V = 0$  is a good approximation, although  $\theta_S = 0$  is doubtful for the low-lying resonances. The terms that vanish in the ideal mixing case are OZI-suppressed.

One consequence of the OZI suppression is that when we consider the full production process, namely  $\gamma\gamma \rightarrow$

vertex	general mixing	$\theta_V = 0$	$\theta_V = \theta_S = 0$
$\rho^0 \rho^0 \rightarrow f_0$	$\cos \theta_S / \sqrt{2}$	$\cos \theta_S / \sqrt{2}$	$1/\sqrt{2}$
$\rho^0 \rho^0 \rightarrow f'_0$	$-\sin \theta_S / \sqrt{2}$	$-\sin \theta_S / \sqrt{2}$	0
$\rho^0 \omega, \omega \rho^0 \rightarrow a_0$	$\cos \theta_V / \sqrt{2}$	$1/\sqrt{2}$	$1/\sqrt{2}$
$\rho^0 \phi, \phi \rho^0 \rightarrow a_0$	$-\sin \theta_V / \sqrt{2}$	0	0
$\omega \omega \rightarrow f_0$	$\cos^2 \theta_V \cos \theta_S / \sqrt{2} + \sin^2 \theta_V \sin \theta_S$	$\cos \theta_S / \sqrt{2}$	$1/\sqrt{2}$
$\omega \omega \rightarrow f'_0$	$-\cos^2 \theta_V \sin \theta_S / \sqrt{2} + \sin^2 \theta_V \cos \theta_S$	$-\sin \theta_S / \sqrt{2}$	0
$\omega \phi \rightarrow f_0$	$\sin \theta_V \cos \theta_V (-\cos \theta_S / \sqrt{2} + \sin \theta_S)$	0	0
$\omega \phi \rightarrow f'_0$	$\sin \theta_V \cos \theta_V (\sin \theta_S / \sqrt{2} + \cos \theta_S)$	0	0
$\phi \phi \rightarrow f_0$	$\sin^2 \theta_V \cos \theta_S / \sqrt{2} + \cos^2 \theta_V \sin \theta_S$	$\sin \theta_S$	0
$\phi \phi \rightarrow f'_0$	$-\sin^2 \theta_V \sin \theta_S / \sqrt{2} + \cos^2 \theta_V \cos \theta_S$	$\cos \theta_S$	1

**Table 1.** The  $VVS$  coupling coefficients. The overall symmetry factor 2 has been suppressed. The vertexes not listed here are forbidden by isospin conservation, so that we have:  $g_{\rho^0 \rho^0 a_0} = g_{\rho^0 \omega f_0} = g_{\rho^0 \omega f'_0} = g_{\rho^0 \phi f_0} = g_{\rho^0 \phi f'_0} = g_{\omega \omega a_0} = g_{\omega \phi a_0} = g_{\phi \phi a_0} = 0$ . We list the general case as well as the ‘ideal mixing’ case corresponding to  $\theta_V = 0$  and to  $\theta_V = \theta_S = 0$ .

$V_1 V_2$  with the vector mesons in the final state, the channels which necessarily involve OZI-suppressed interaction are suppressed, so that we expect:

$$\begin{aligned} & \sigma(\gamma\gamma \rightarrow \rho^0 \rho^0), \sigma(\gamma\gamma \rightarrow \omega\omega) \\ & > \sigma(\gamma\gamma \rightarrow \rho^0 \omega) > \sigma(\gamma\gamma \rightarrow \phi\phi) \\ & \gg \sigma(\gamma\gamma \rightarrow \rho^0 \phi), \sigma(\gamma\gamma \rightarrow \omega\phi). \end{aligned} \quad (18)$$

The reasoning goes as follows. Let us first emphasize that this is for the entire  $s$ -channel production process as given by the factorization of eqn. (7). The photons first couple to the appropriate vector boson, which fuse together into a (scalar) resonance, then finally decay into the states given above. In the ideal mixing case,  $\rho^0 \rho^0$  and  $\omega\omega$  both come from  $f$  decay with equal strength, so that  $\rho^0 \rho^0$  and  $\omega\omega$  are approximately equal.  $\rho^0 \omega$  can come from  $a$ , but  $a$  production is slightly smaller than  $f$  because of the ratio of  $\rho^0$  and  $\omega$  contents of the photon.  $\phi\phi$  is suppressed because  $f'$  is less abundant than  $f$ , that is,  $\rho^0 \rho^0 \rightarrow f$  is the dominant resonance production subprocess.

## 2.2 Meson pair production

We now turn to the decay subprocess. Let us first consider the production of pseudo-scalar mesons. These are in the nonet representation of eqn. (12).

The relevant coefficients can be obtained by the diagonal,  $a = b$ , part of:

$$\frac{1}{2} S_a^b (P_b^c P_c^a + P_c^a P_b^c). \quad (19)$$

We list them in tab. 2.

Again, those modes that are OZI suppressed are accompanied by factor  $\sin \theta_S$  or  $\sin \theta_P$ . However, since  $\theta_P$  is now considerably large,  $\approx -39$  degrees [17], the suppression factor is only moderate.  $\theta_S$  is also considerably large for the spin-0 bosons [18] although possibly not for the higher-spin excitations of  $a$ ,  $f$  and  $f'$ .

We see that, after including the identical particle factor of 1/2 for the  $\pi^0 \pi^0$  cross section:

$$\sigma(\gamma\gamma \rightarrow \pi^+ \pi^-) = 2\sigma(\gamma\gamma \rightarrow \pi^0 \pi^0), \quad (20)$$

regardless of the mixing angles or production dynamics. We also see that the channels:

$$\gamma\gamma \rightarrow \pi^0 \eta, \pi^0 \eta', \quad (21)$$

can only proceed via  $s$ -channel isovector  $a$ , so that the observation of these processes would be interesting to confirm the presence of the isovector channel. The magnitude of these channels is related to the difference of the kaon amplitudes, i.e.:

$$\begin{aligned} & \left| \mathcal{A}(\gamma\gamma \rightarrow K^+ K^-) - \mathcal{A}(\gamma\gamma \rightarrow K^0 \bar{K}^0) \right|^2 \\ & = \left| \mathcal{A}(\gamma\gamma \rightarrow \pi^0 \eta) \right|^2 + \left| \mathcal{A}(\gamma\gamma \rightarrow \pi^0 \eta') \right|^2, \end{aligned} \quad (22)$$

In particular, when the  $K^+ K^-$  cross section dominates over  $K^0 \bar{K}^0$ , and when  $W_{\gamma\gamma}$  is sufficiently above the  $\pi^0 \eta'$  threshold, we obtain:

$$\sigma(\gamma\gamma \rightarrow K^+ K^-) \approx \sigma(\gamma\gamma \rightarrow \pi^0 \eta) + \sigma(\gamma\gamma \rightarrow \pi^0 \eta'). \quad (23)$$

This should be tested experimentally. However, we shall show later that the ratio between the  $K^+ K^-$  and  $K^0 \bar{K}^0$  amplitudes is expected to be at most 4, and hence omitting the  $K^0 \bar{K}^0$  amplitude contribution is not a good approximation. One possible assumption would be that the two cross sections only differ by a real constant factor. The cross section would then be scaled by:

$$\begin{aligned} & \sigma(\gamma\gamma \rightarrow K^+ K^-) \longrightarrow \\ & \sigma(\gamma\gamma \rightarrow K^+ K^-) \times \left( 1 - \sqrt{\frac{\sigma(\gamma\gamma \rightarrow K^0 \bar{K}^0)}{\sigma(\gamma\gamma \rightarrow K^+ K^-)}} \right)^2 \end{aligned} \quad (24)$$

Similarly, for the sum of the  $K^+ K^-$  and  $K^0 \bar{K}^0$  amplitudes, we find that:

$$\begin{aligned} & 2 \left[ \mathcal{A}(\gamma\gamma \rightarrow K^+ K^-) + \mathcal{A}(\gamma\gamma \rightarrow K^0 \bar{K}^0) \right] \\ & = \mathcal{A}(\gamma\gamma \rightarrow \eta\eta) + \mathcal{A}(\gamma\gamma \rightarrow \eta'\eta'). \end{aligned} \quad (25)$$

However, this equality would be difficult to test experimentally, unless it is found, for instance, that  $\eta\eta$  dominates over  $\eta'\eta'$  when sufficiently above the threshold. In

final state	$a_0$	$f_0$	$f'_0$
$\pi^+\pi^-$	0	$\cos\theta_S\sqrt{2}$	$-\sin\theta_S\sqrt{2}$
$K^+K^-$	$\frac{1}{\sqrt{2}}$	$\frac{\cos\theta_S}{\sqrt{2}} + \sin\theta_S$	$-\frac{\sin\theta_S}{\sqrt{2}} + \cos\theta_S$
$\pi^0\pi^0$	0	$\cos\theta_S\sqrt{2}$	$-\sin\theta_S\sqrt{2}$
$K^0\bar{K}^0$	$-\frac{1}{\sqrt{2}}$	$\frac{\cos\theta_S}{\sqrt{2}} + \sin\theta_S$	$-\frac{\sin\theta_S}{\sqrt{2}} + \cos\theta_S$
$\pi^0\eta, \eta\pi^0$	$\cos\theta_P\sqrt{2}$	0	0
$\pi^0\eta', \eta'\pi^0$	$-\sin\theta_P\sqrt{2}$	0	0
$\eta\eta$	0	$2\left(\cos^2\theta_P\frac{\cos\theta_S}{\sqrt{2}} + \sin^2\theta_P\sin\theta_S\right)$	$2\left(-\cos^2\theta_P\frac{\sin\theta_S}{\sqrt{2}} + \sin^2\theta_P\cos\theta_S\right)$
$\eta\eta'$	0	$2\sin\theta_P\cos\theta_P\left(-\frac{\cos\theta_S}{\sqrt{2}} + \sin\theta_S\right)$	$2\sin\theta_P\cos\theta_P\left(\frac{\sin\theta_S}{\sqrt{2}} + \cos\theta_S\right)$
$\eta'\eta'$	0	$2\left(\sin^2\theta_P\frac{\cos\theta_S}{\sqrt{2}} + \cos^2\theta_P\sin\theta_S\right)$	$2\left(-\sin^2\theta_P\frac{\sin\theta_S}{\sqrt{2}} + \cos^2\theta_P\cos\theta_S\right)$

**Table 2.** The *SPP* coupling coefficients.

this case, the relation would reduce to:

$$\sigma(\gamma\gamma \rightarrow K^+K^-) \approx \frac{1}{2}\sigma(\gamma\gamma \rightarrow \eta\eta). \quad (26)$$

The  $\frac{1}{2}$  factor on the right-hand side comes from the combination of the factor 2 in eqn. (25) and the factor  $\frac{1}{2}$  for identical particle production. Again, we can adjust for the error in neglecting the sub-leading amplitudes by a scaling similar to eqn. (24) but with the minus sign in the brackets replaced by a plus sign.

The above argument holds regardless of the production subprocess  $VV \rightarrow S$ . Let us now consider the inclusion of the production subprocess. This is obtained by referring to eqn. (7). We adopt ideal mixing for the vector mesons so that  $\theta_V = 0$ . The result, for  $\gamma\gamma \rightarrow K^+K^-, K^0\bar{K}^0, \pi^+\pi^-$ , and  $\pi^0\pi^0$  are:

$$\begin{aligned} \mathcal{A}(\gamma\gamma \rightarrow K^+K^-) &= F(f_0) \left( \frac{\cos\theta_S}{\sqrt{2}} + \sin\theta_S \right) \left( \frac{5}{9} \frac{\cos\theta_S}{\sqrt{2}} + \frac{\delta}{9} \sin\theta_S \right) \\ &+ F(f'_0) \left( \frac{\sin\theta_S}{\sqrt{2}} - \cos\theta_S \right) \left( \frac{5}{9} \frac{\sin\theta_S}{\sqrt{2}} - \frac{\delta}{9} \cos\theta_S \right) \\ &+ \frac{1}{6}F(a_0), \end{aligned} \quad (27)$$

$$\begin{aligned} \mathcal{A}(\gamma\gamma \rightarrow K^0\bar{K}^0) &= F(f_0) \left( \frac{\cos\theta_S}{\sqrt{2}} + \sin\theta_S \right) \left( \frac{5}{9} \frac{\cos\theta_S}{\sqrt{2}} + \frac{\delta}{9} \sin\theta_S \right) \\ &+ F(f'_0) \left( \frac{\sin\theta_S}{\sqrt{2}} - \cos\theta_S \right) \left( \frac{5}{9} \frac{\sin\theta_S}{\sqrt{2}} - \frac{\delta}{9} \cos\theta_S \right) \\ &- \frac{1}{6}F(a_0), \end{aligned} \quad (28)$$

$$\begin{aligned} \mathcal{A}(\gamma\gamma \rightarrow \pi^+\pi^-) &= F(f_0) \cos\theta_S \left( \frac{5}{9} \cos\theta_S + \frac{\delta}{9} \sqrt{2} \sin\theta_S \right) \\ &+ F(f'_0) \sin\theta_S \left( \frac{5}{9} \sin\theta_S - \frac{\delta}{9} \sqrt{2} \cos\theta_S \right), \end{aligned} \quad (29)$$

$$\begin{aligned} \mathcal{A}(\gamma\gamma \rightarrow \pi^0\pi^0) &= F(f_0) \cos\theta_S \left( \frac{5}{9} \cos\theta_S + \frac{\delta}{9} \sqrt{2} \sin\theta_S \right) \end{aligned}$$

$$+ F(f'_0) \sin\theta_S \left( \frac{5}{9} \sin\theta_S - \frac{\delta}{9} \sqrt{2} \cos\theta_S \right). \quad (30)$$

$\delta$  is defined below eqn. (8). The above expressions simplify in the case  $\theta_S = 0$ . As mentioned earlier, this becomes acceptable for the higher-spin excitations of  $f, a$ , and  $f'$ . We then have:

$$\begin{aligned} \mathcal{A}(\gamma\gamma \rightarrow K^+K^-) &= \frac{1}{18} [5F(f_0) + 2\delta F(f'_0) + 3F(a_0)], \end{aligned} \quad (31)$$

$$\begin{aligned} \mathcal{A}(\gamma\gamma \rightarrow K^0\bar{K}^0) &= \frac{1}{18} [5F(f_0) + 2\delta F(f'_0) - 3F(a_0)], \end{aligned} \quad (32)$$

$$\mathcal{A}(\gamma\gamma \rightarrow \pi^+\pi^-) = \frac{5}{9}F(f_0), \quad (33)$$

$$\mathcal{A}(\gamma\gamma \rightarrow \pi^0\pi^0) = \frac{5}{9}F(f_0). \quad (34)$$

We may simplify further by the approximation  $F(f_0) = F(a_0)$  and absorbing the difference between  $F(f'_0)$  and  $F(f_0)$  in the coefficient  $\delta$ . Under these conditions, i.e.,  $F(a) = F(f) = F(f')$  for arbitrary  $\delta$ , it turns out that all dependence on  $\theta_S$  cancels automatically, so that ideal mixing becomes a redundant assumption. We obtain, at the amplitude level:

$$K^+K^- : K^0\bar{K}^0 : \pi^+\pi^- : \pi^0\pi^0 = 4 + \delta : 1 + \delta : 5 : 5. \quad (35)$$

In particular, for the ratio of the  $\gamma\gamma \rightarrow K^+K^-$  and  $K_S K_S$  cross sections, we have:

$$\frac{\sigma(\gamma\gamma \rightarrow K^+K^-)}{\sigma(\gamma\gamma \rightarrow K_S K_S)} \equiv 2 \frac{\sigma(\gamma\gamma \rightarrow K^+K^-)}{\sigma(\gamma\gamma \rightarrow K^0\bar{K}^0)} = 2 \left( \frac{4 + \delta}{1 + \delta} \right)^2. \quad (36)$$

The conventional charge-counting argument [13] corresponds to  $\delta = 1$  and therefore gives 25/2. On the other hand, the complete suppression of  $f'$  gives rise to 32. Since physically we expect  $\delta$  to be positive definite, we obtain the following inequality:

$$12.5 < \frac{\sigma(\gamma\gamma \rightarrow K^+K^-)}{\sigma(\gamma\gamma \rightarrow K_S K_S)} < 32. \quad (37)$$

The upper limit of this equation seems to be satisfied by the currently available data [9], within the statistical errors. The closeness of the observed ratio at high energy with the limiting value 32 indicates the suppression of the strangeness coupling in this region. The lower limit seems to be violated at lower energies [9]. One possible reason is that, in this region, there is dominant contribution from  $f'$  corresponding to the possibility  $\delta > 1$ , but another possible reason is that, as we shall argue later, long-distance interaction tends to respect isospin invariance, and so the  $a$  coupling is suppressed.

Another quantity that may be interesting is the ratio of the  $K^+K^-$  and  $\pi^+\pi^-$  cross sections. We obtain:

$$\frac{\sigma(\gamma\gamma \rightarrow K^+K^-)}{\sigma(\gamma\gamma \rightarrow \pi^+\pi^-)} = \left(\frac{4+\delta}{5}\right)^2. \quad (38)$$

We therefore expect that sufficiently above the threshold, the  $K^+K^-$  cross section is smaller than the  $\pi^+\pi^-$  cross section by up to a factor of 16/25.

If the suppression factor  $\delta$  is indicative only of the resonance structure denoted by  $F(f')$ , and not the coupling, of  $f'$ , it then follows that the  $\delta$  obtained by the comparison of these cross sections should be approximately the same as the  $\delta$  obtained by the comparison of the  $K^+K^-$  and  $K_S K_S$  in the same kinematic range, i.e., the same  $W_{\gamma\gamma}$  and  $\cos\theta^*$  intervals. This should be tested experimentally.

### 2.3 Baryon pair production

Baryons belong to the  $\mathbf{3} \otimes \mathbf{3} \otimes \mathbf{3}$  representation, which is decomposed as:

$$\mathbf{3} \otimes \mathbf{3} \otimes \mathbf{3} = \mathbf{10}_S \oplus \mathbf{8}_{MS} \oplus \mathbf{8}_{MA} \oplus \mathbf{1}_A. \quad (39)$$

Out of these, phenomenologically the most relevant are the  $1/2^+$  baryons in the octet representation. The subscripts **MS** and **MA** stand for mixed symmetric and mixed antisymmetric, respectively. We write them as:

$$\mathbf{8}_{MS} = B_{(a,b)c}, \quad (40)$$

$$\mathbf{8}_{MA} = B_{[a,b]c}. \quad (41)$$

Curly brackets in the subscript represent the symmetric sum and square brackets represent the antisymmetric sum, so that:

$$B_{(a,b)c} = B_{(b,a)c}, \quad B_{[a,b]c} = -B_{[b,a]c}. \quad (42)$$

Furthermore,  $B_{[a,b]c}$  also satisfy the Jacobi identity:

$$B_{[a,b]c} + B_{[b,c]a} + B_{[c,a]b} = 0. \quad (43)$$

The symmetric and antisymmetric representations contain the same physical states, and they are related by:

$$B_b^a = \epsilon^{acd} B_{(d,b)c} = \frac{1}{2} \epsilon^{acd} B_{[c,d]b}, \quad (44)$$

where  $\epsilon^{acd}$  is the Levi-Civita tensor with the convention  $\epsilon^{123} = 1$ .  $B_b^a$  is the octet matrix. We first write down the content of  $B_{[a,b]c}$  explicitly:

$$\begin{aligned} B_{[1,2]1} &= p, & B_{[1,2]2} &= n, & B_{[1,2]3} &= -2A/\sqrt{6}, \\ B_{[1,3]1} &= -\Sigma^+, & B_{[1,3]2} &= \Sigma^0/\sqrt{2} - A/\sqrt{6}, & B_{[1,3]3} &= -\Xi^0, \\ B_{[2,3]1} &= \Sigma^0/\sqrt{2} + A/\sqrt{6}, & B_{[2,3]2} &= \Sigma^-, & B_{[2,3]3} &= -\Xi^-. \end{aligned} \quad (45)$$

The octet matrix  $B_b^a$  is then:

$$B_b^a = \begin{pmatrix} \Sigma^0/\sqrt{2} + A/\sqrt{6} & \Sigma^+ & p \\ \Sigma^- & -\Sigma^0/\sqrt{2} + A/\sqrt{6} & n \\ -\Xi^- & \Xi^0 & -2A/\sqrt{6} \end{pmatrix}. \quad (46)$$

There are three possibilities for evaluating the baryon-baryon-meson  $SBB$  coupling. We can work in terms of  $B_{(a,b)c}$ ,  $B_{[a,b]c}$  or  $B_b^a$ . Here we adopt the following notation:

$$\frac{1}{2} \alpha \bar{B}^{[c,d]a} B_{[c,d]b} M_a^b + \beta \bar{B}^{[a,c]d} B_{[b,c]d} M_a^b. \quad (47)$$

$\alpha$  and  $\beta$  are adjustable parameters satisfying [19]:

$$\alpha \approx 5\beta. \quad (48)$$

This relation comes from the approximate flavour  $SU(3)$  symmetry for baryon-meson strong coupling constants. On the other hand, for the naive charge-counting argument to work, we need to impose  $\alpha = \beta$ . This point will be demonstrated by an example later.

We can now tabulate the relevant coupling constants in terms of  $\alpha$  and  $\beta$ , and these are listed in tab. 3.

We can consider forming equalities similar to eqns. (22) and (25). In particular, we can make use of the ratios of  $a_0$  couplings:

$$\begin{aligned} &\mathcal{A}(\gamma\gamma \rightarrow p\bar{p}) - \mathcal{A}(\gamma\gamma \rightarrow n\bar{n}) : \\ &\mathcal{A}(\gamma\gamma \rightarrow \Sigma^+\bar{\Sigma}^+) - \mathcal{A}(\gamma\gamma \rightarrow \Sigma^-\bar{\Sigma}^-) : \\ &\mathcal{A}(\gamma\gamma \rightarrow \Xi^0\bar{\Xi}^0) - \mathcal{A}(\gamma\gamma \rightarrow \Xi^-\bar{\Xi}^-) : \\ &\mathcal{A}(\gamma\gamma \rightarrow \Sigma^0\bar{\Lambda}) \\ &= \alpha : \alpha + \beta : \beta : \frac{\alpha - \beta}{2\sqrt{3}}. \end{aligned} \quad (49)$$

However, these will be difficult to verify experimentally. This is partly because some final states, for example  $n\bar{n}$ , are difficult to measure, and partly because we do not expect in any of the pairs of reactions above that either of the two amplitudes would become sufficiently dominant over the other that the other can be neglected.

It is hence more helpful to make an estimation analogous to eqn. (35). For example, the  $p\bar{p}$  amplitude is given, for  $\theta_V = 0$ , by:

$$\begin{aligned} &\mathcal{A}(\gamma\gamma \rightarrow p\bar{p}) \\ &= \frac{5}{18} (\alpha + 2\beta) [\cos^2 \theta_S F(f_0) + \delta \sin^2 \theta_S F(f_0')] \\ &+ \frac{\alpha}{6} F(a_0). \end{aligned} \quad (50)$$

final state	$a_0$	$f_0$	$f'_0$
$p\bar{p}$	$\alpha/\sqrt{2}$	$(\alpha + 2\beta) \cos \theta_S/\sqrt{2}$	$-(\alpha + 2\beta) \sin \theta_S/\sqrt{2}$
$n\bar{n}$	$-\alpha/\sqrt{2}$	$(\alpha + 2\beta) \cos \theta_S/\sqrt{2}$	$-(\alpha + 2\beta) \sin \theta_S/\sqrt{2}$
$\Sigma^+\bar{\Sigma}^+$	$\frac{\alpha+\beta}{\sqrt{2}}$	$(\alpha + \beta) \cos \theta_S/\sqrt{2} + \beta \sin \theta_S$	$-(\alpha + \beta) \sin \theta_S/\sqrt{2} + \beta \cos \theta_S$
$\Sigma^0\bar{\Sigma}^0$	0	$(\alpha + \beta) \cos \theta_S/\sqrt{2} + \beta \sin \theta_S$	$-(\alpha + \beta) \sin \theta_S/\sqrt{2} + \beta \cos \theta_S$
$\Sigma^-\bar{\Sigma}^-$	$-\frac{\alpha+\beta}{\sqrt{2}}$	$(\alpha + \beta) \cos \theta_S/\sqrt{2} + \beta \sin \theta_S$	$-(\alpha + \beta) \sin \theta_S/\sqrt{2} + \beta \cos \theta_S$
$\Lambda\bar{\Lambda}$	0	$\frac{\alpha+5\beta}{3\sqrt{2}} \cos \theta_S + \frac{2\alpha+\beta}{3} \sin \theta_S$	$-\frac{\alpha+5\beta}{3\sqrt{2}} \sin \theta_S + \frac{2\alpha+\beta}{3} \cos \theta_S$
$\Xi^0\bar{\Xi}^0$	$\beta/\sqrt{2}$	$(\alpha + \beta) \sin \theta_S + \beta \cos \theta_S/\sqrt{2}$	$(\alpha + \beta) \cos \theta_S - \beta \sin \theta_S/\sqrt{2}$
$\Xi^-\bar{\Xi}^-$	$-\beta/\sqrt{2}$	$(\alpha + \beta) \sin \theta_S + \beta \cos \theta_S/\sqrt{2}$	$(\alpha + \beta) \cos \theta_S - \beta \sin \theta_S/\sqrt{2}$
$\Sigma^0\bar{\Lambda}, \Lambda\bar{\Sigma}^0$	$\frac{\alpha-\beta}{\sqrt{6}}$	0	0

**Table 3.** The  $SB\bar{B}$  coupling coefficients.

As before, by taking  $\theta_S = 0$ ,  $F(f_0) = F(a_0)$  and absorbing the difference between  $F(f_0)$  and  $F(f'_0)$  into the coefficient  $\delta$ , we arrive at:

$$\mathcal{A}(\gamma\gamma \rightarrow p\bar{p}) \approx \frac{F}{9}(4\alpha + 5\beta). \quad (51)$$

We repeat the same exercise for the other production modes and obtain results listed in tab. 4.

The statement made earlier about naive charge-counting in the case  $\alpha = \beta$  can now be demonstrated explicitly. For example, the ratio of the  $p\bar{p}$  and  $n\bar{n}$  amplitudes is given by:

$$\frac{8 + 10}{2 + 10} = \frac{3}{2} = \frac{1^2 + 2^2 + 2^2}{1^2 + 1^2 + 2^2}. \quad (52)$$

The ratios of cross sections sufficiently above the threshold region are given by the square of the coefficients listed in tab. 4, so that, for instance:

$$\frac{\sigma(\gamma\gamma \rightarrow p\bar{p})}{\sigma(\gamma\gamma \rightarrow \Sigma^0\bar{\Sigma}^0)} \approx \left( \frac{8\alpha + 10\beta}{5\alpha + (5 + 2\delta)\beta} \right)^2. \quad (53)$$

This quantity comes out to be between  $\sim 2.4$  and  $\sim 2.7$  for  $\alpha = 5\beta$  and  $0 < \delta < 1$ . The measurement of the  $\Xi^0\bar{\Xi}^0$ , or  $\Xi^-\bar{\Xi}^-$ , cross section would be particularly interesting because of the sensitivity to  $\delta$ . From the discussion of pseudo-scalar meson pair production, we expect that  $\delta$  is small, so that this cross section would be suppressed by factor  $\sim (50/8)^2 \sim 40$  compared to the  $p\bar{p}$  cross section.

### 3 Long- and short-distance dynamics

Let us model the short-distance amplitude as a scaling contribution:

$$\mathcal{A} \propto \frac{s^{4-K/2}}{(t - M_1^2)(u - M_2^2)}. \quad (54)$$

$K$  is as appearing in eqn. (1). We take the two masses  $M_1$  and  $M_2$  to be the corresponding hadron masses as opposed to, for instance, some appropriate quark masses. The contribution of these mass terms is negligible in any case in the region of interest. This expression gives rise to

the angular distribution  $\approx (1 - \cos^2 \theta)^{-2}$  which is characteristic of single quark exchange, or more generally light particle exchange, in the  $t$ -channel. This angular distribution would be valid at high-energy, and the scaling behaviour of eqn. (1) implies that the angular distribution must remain the same at low-energy.

To this, we add a long-distance pole(-resonance) contribution which has the Regge limiting form:

$$\mathcal{A} \propto \Gamma(\ell - \alpha(t)) (1 + \tau \exp(-i\pi\alpha(t))) (\alpha' s)^{\alpha(t)} + (t \leftrightarrow u), \quad (55)$$

The linear trajectory is parametrized  $\alpha(t) = \alpha(0) + \alpha't$  as usual, with  $\alpha' \approx 0.9 \text{ GeV}^{-2}$ .  $\ell$  is the lowest spin of the trajectory, and  $\tau = \pm 1$  is the signature. For baryons, the signature term is modified to [23]:

$$1 + \tau \exp(-i\pi(\alpha(t) - 1/2)). \quad (56)$$

It is found [21] that a simple Regge expression similar to eqn. (55) yields characteristic behaviour in the central region  $\cos \theta^* \approx 0$  that is in accordance with the  $\gamma\gamma \rightarrow p\bar{p}$  data just above the threshold. This may seem surprising at first sight, but is reasonable considering that the (Regge) pole amplitude and the resonance amplitude are related by (semi-local) duality [20]. After integrating over the resonances, the behaviour of the two amplitudes is similar. In particular, this method works well in the case of  $p\bar{p}$  since the cross section is a smooth function of  $W_{\gamma\gamma}$  and no trace of resonances is seen. For  $K^+K^-$ , the resonance structure is still seen, so that we may, for instance, replace the Regge amplitude with a resonance-pole dual amplitude of the Veneziano model [22].

#### 3.1 Baryon pair production

Let us first consider  $p\bar{p}$  production. In eqn. (54), we set  $K = 8$ . In eqn. (55) with the modification of eqn. (56), we set  $\ell = \frac{1}{2}$ . As for the trajectories, ref. [23], the leading  $S = 0$  contributions, the  $N/\Delta$ , have the following parametrization:

$$N_\alpha : \alpha(t) = -0.34 + 0.99t, \quad (57)$$

$$N_\gamma : \alpha(t) = -0.63 + 0.89t, \quad (58)$$

$$N_\beta : \alpha(t) = 0 + 0.9t, \quad (59)$$

$$\Delta_\delta : \alpha(t) = 0.07 + 0.92t. \quad (60)$$

final state	$18A/F$	$\alpha = 5, \beta = 1, \delta = 1$	$\delta = 0$
$p\bar{p}$	$8\alpha + 10\beta$	50	50
$n\bar{n}$	$2\alpha + 10\beta$	20	20
$\Sigma^+\bar{\Sigma}^+$	$8\alpha + (8 + 2\delta)\beta$	50	48
$\Sigma^0\bar{\Sigma}^0$	$5\alpha + (5 + 2\delta)\beta$	32	30
$\Sigma^-\bar{\Sigma}^-$	$2\alpha + (2 + 2\delta)\beta$	14	12
$\Lambda\bar{\Lambda}$	$(5 + 4\delta)\alpha/3 + (25 + 2\delta)\beta/3$	24	16.67
$\Xi^0\bar{\Xi}^0$	$2\delta\alpha + (8 + 2\delta)\beta$	20	8
$\Xi^-\bar{\Xi}^-$	$2\delta\alpha + (2 + 2\delta)\beta$	14	2
$\Sigma^0\bar{\Lambda}, \Lambda\bar{\Sigma}^0$	$(\alpha - \beta)\sqrt{3}$	6.93	6.93

**Table 4.** The limiting behaviour of  $\gamma\gamma \rightarrow B\bar{B}$  amplitudes.

$N_\alpha$  and  $N_\beta$  are signature even whereas  $N_\gamma$  and  $N_\delta$  are signature odd.  $N$  are isospin 1/2 and  $\Delta$  are isospin 3/2, as usual. Both exchanges are allowed, although  $\Delta$  exchange can only take place in  $\rho\rho \rightarrow p\bar{p}$  and not in the other sub-processes.

In principle, we should include all four contributions. In practice, however, we found phenomenologically that the inclusion of just one trajectory, the  $N_\beta$  trajectory, is sufficient.

For the explicit  $\alpha'$  in eqn. (55), as opposed to the  $\alpha'$  implicit in the trajectory  $\alpha(t)$ , we adopt  $0.9 \text{ GeV}^{-2}$ .

In fig. 3, we show the scaling amplitude, the Regge amplitude, and the sum of the two. We first fix the normalization of the scaling contribution by fitting by the eye with the data at  $W_{\gamma\gamma}$  near 4 GeV. We then adjust the Regge contribution so that the sum of the two terms fits the integrated cross section.

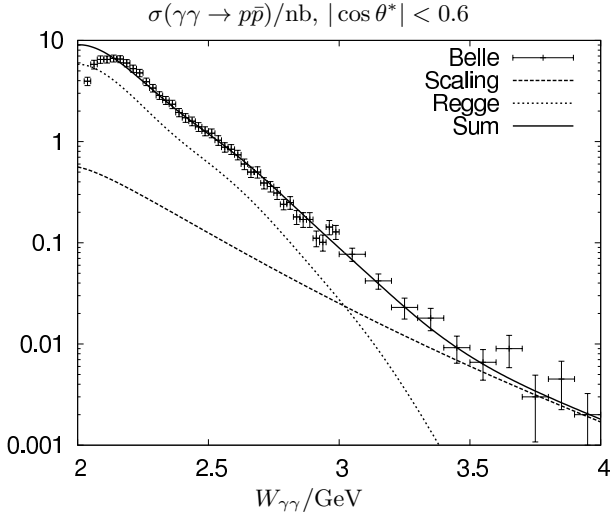


**Fig. 3.** The  $\gamma\gamma \rightarrow p\bar{p}$  integrated cross section in the region  $|\cos\theta^*| < 0.6$ . We show the Belle result against three theoretical results: scaling based on the quark-counting rule, the Regge amplitude, and the sum of the two. The vertical error-bars only includes the statistical uncertainty.

There is good agreement with the data, except in the region just above the threshold. Even this region shows

improvement compared with our previous calculation in ref. [21], where the signature term was neglected. We note that by further modifying the signature term by the artificial substitution  $\tau \rightarrow -i$ , we were able to obtain the fall-off near threshold seen in the real data. This suggests the possibility that the inclusion of other trajectories and/or resonances with appropriate strengths may change the threshold behaviour.

The angular distributions are shown in fig. 4. The shifting of the peak of the central angular distribution from the  $\cos\theta \approx 0$  region to the forward region occurs slightly faster (about 100 MeV faster) in the theoretical curve than in the experimental data. However, the overall trend is in fair agreement with that seen in the experiment.

Having achieved this level of agreement, it becomes desirable to be able to extend our results to the case of other baryons, for instance  $\Lambda$  and  $\Sigma^0$  [24,25]. However, there is no good method for estimating the Regge couplings [15]. On the other hand, we expect that for all baryons, the Regge contributions dominate over the scaling contribution, since the Regge contribution is expected to be more insensitive to the type of the baryon [15], whereas the scaling contribution, from tab. 4, is always smaller than the proton pair case.

As noted in ref. [21], just above the threshold region, we expect invariance under  $u \leftrightarrow d$ , as opposed to the  $d \leftrightarrow s$  symmetry that follows from the perturbative approaches [13,26]. This implies, in the  $s$ -channel picture, the suppression of isovector  $a$  component. Hence  $\Sigma^0\bar{\Lambda}$  production would be suppressed.

The size of the scaling contribution to each baryon pair can be estimated from tab. 4, but this is, as seen in the above results, small. The more central, or the higher-energy region, is expected to have a more short-distance character and so the argument of sec. 2 can be applied.

### 3.2 Meson pair production

We now consider meson pair photoproduction. In eqn. (54), we set  $K = 6$ . In eqn. (55), we set  $\ell = 1$ .

The signature  $\tau$  in eqn. (55) can be  $\pm 1$  depending on the spin of the trajectory. However, unlike in the baryonic case discussed above, we have spin-degenerate trajectories with  $\tau = +1$  and  $\tau = -1$ .  $\tau = +1$  corresponds to the



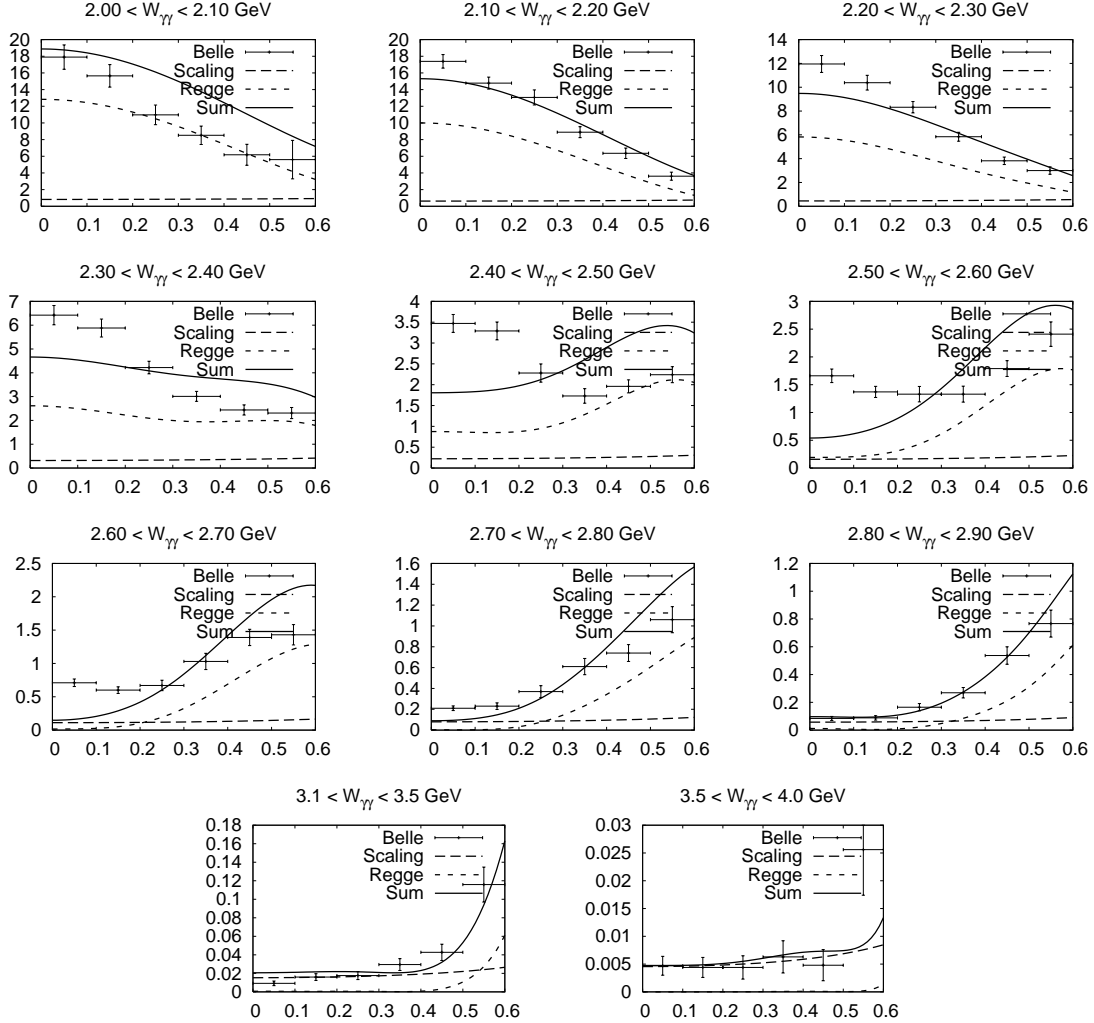


**Fig. 4.** The angular distribution of  $\gamma\gamma \rightarrow p\bar{p}$ . The results of three theoretical model calculations are compared against the experimental data from ref. [1].

exchange of even-spin mesons:

$$\mathcal{A} \propto \Gamma(1 - \alpha(t)) (1 + \exp(-i\pi\alpha(t))) (\alpha' s)^{\alpha(t)}. \quad (61)$$

The odd-spin mesons have  $\tau = -1$  and:

$$\mathcal{A} \propto \Gamma(1 - \alpha(t)) (1 - \exp(-i\pi\alpha(t))) (\alpha' s)^{\alpha(t)}. \quad (62)$$

Adding together the contributions of degenerate trajectories, the contribution of the signature term in general tends to cancel. In the limiting case of perfect cancellation, there are two possibilities:

1. The two amplitude add with the same sign, leading to the cancellation of  $\exp(-i\pi\alpha(t))$ . This corresponds to the cancellation of the handbag diagrams in fig. 2.
2. The two amplitudes add with the opposite sign, leading to the cancellation of the constant-phase term. This corresponds to the the cancellation of the cat's-ears diagram in fig. 2.

Let us denote these respectively as ‘Regge cat’s-ears’ and ‘Regge handbag’. It turns out that the plateau structure of the  $K^+K^-$  integrated cross section is only reproduced in the ‘Regge handbag’ case, since a rotating phase is necessary to yield non-trivial interference with the scaling contribution.

Let us therefore consider the ‘Regge handbag’ case. Here, we can write the combined amplitude as a  $s - t$  dual amplitude. Using the simple Veneziano amplitude of ref. [21], we are able to simulate both the resonance and the pole regions with the expression:

$$\mathcal{A} \propto \frac{\Gamma(1 - \alpha(t))\Gamma(1 - \alpha(s))}{\Gamma(1 - \alpha(t) - \alpha(s))} + (u \leftrightarrow t), \quad (63)$$

from which we can recover the Regge amplitude by the application of the Stirling factorial approximation. Because of the resonance–pole duality, the discussion of the preceding sec. 2 holds. This has the implication that relations between amplitudes such as eqns. (22) and (25) are satisfied.

We fit the scaling amplitude by the eye to the data at near 4 GeV. We then study the behaviour of the sum of this amplitude and the parametrization of ref. [21]. The result is shown in fig. 5. The scaling curve fits the data

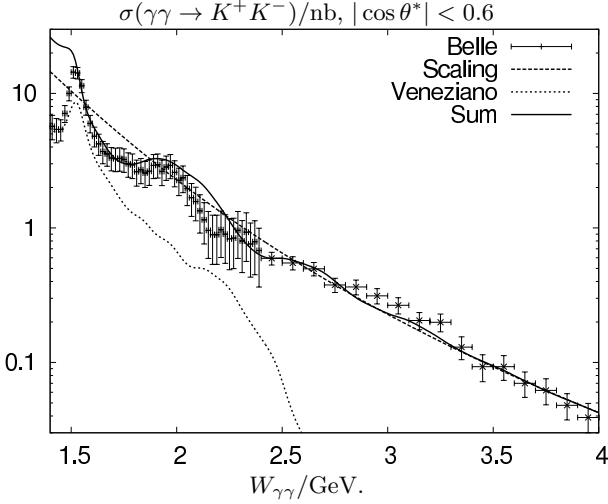


**Fig. 5.**  $\gamma\gamma \rightarrow K^+K^-$  integrated cross section in the region  $|\cos\theta^*| < 0.6$ . The experimental results [2] are compared against scaling, the Veneziano model, and the sum of the two.

reasonably above about 2.5 GeV. Below 2.5 GeV, the behaviour of the integrated cross section is still close to the scaling curve, but this is accidental since the behaviour of the angular distribution is far from that parametrized by eqn. (54). On the other hand, the Veneziano amplitude by itself provides a semi-quantitative description of the data below about 2 GeV although the plateaus just below and above 2 GeV are not reproduced.

The sum of the two amplitudes shows striking resemblance to the real data, except below 1.5 GeV. In particular, this reproduces the plateaus. These come from the non-trivial interference between the long-distance and short-distance contributions to the amplitude, and are, as seen in fig. 5, not correlated directly with the shape of the resonances.

This apparent resemblance with the data is, however, misleading, since the angular distribution does not correctly reproduce the structure of the experimental data. This is seen in fig. 6, which shows the distribution at three representative energy ranges and in the region between 2.00 and 2.20 GeV. For most of the energy range, the sum of the two amplitudes does not yield a better approximation to the angular distribution than either of the two individual contributions.

The plateau structure is weakened but still visible when we adopt the Regge limiting expression of the Veneziano amplitude, as shown in fig. 7. The situation with respect to the angular distribution improves in the Regge limiting case, especially above 2 GeV. This is shown in fig. 8. The improvement in the fit compared with the Veneziano amplitude is mostly due to the reduced size of the Regge

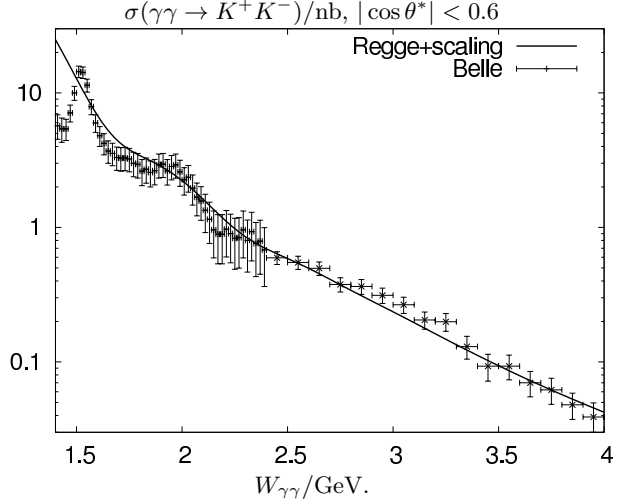


**Fig. 7.**  $\gamma\gamma \rightarrow K^+K^-$  integrated cross section in the region  $|\cos\theta^*| < 0.6$ . The experimental results [2] are compared against the sum of the Regge and scaling amplitudes.

limiting expression compared to the Veneziano amplitude. If the Regge amplitude normalization is modified to more closely resemble that of the Veneziano amplitude, the fit deteriorates.

The angular distribution below 2 GeV is not well reproduced.

Since the Veneziano amplitude by itself fits the distribution well in the low-energy region, it is tempting to introduce a form factor that allows smooth transition between the long-distance and scaling amplitudes. We have experimented with several such possibilities and found that although the fit with the angular distribution improves, it is difficult to obtain the plateau structure of the integrated cross section.

Let us now turn our attention to the  $K_S K_S$  cross section. We make two assumptions for the  $K^0 \bar{K}^0 = K_S K_S + K_L K_L$  cross section with respect to the  $K^+ K^-$  cross section, namely:

1. the scaling amplitude is scaled by a constant factor of  $1/4$ ;
2. the Veneziano amplitude remains the same.

The first implies the complete exclusion of the strange-quark contribution, and the second implies the invariance of the long-distance amplitude with respect to isospin.

The results are shown in fig. 9. The large ratio between  $K^+ K^-$  and  $K_S K_S$  cross sections, as well as the increasing ratio between the two, is reproduced. However, the ratio seems to increase more rapidly in the real data. From our above results of the  $K^+ K^-$  cross section, we expect that the angular distribution may not be reproduced correctly. However, if the long-distance effects are still active in the high-energy range, a model-independent statement is that the angular distribution would be affected, and will not be given by a simple scaling form such as eqn. (54).

We note that for pions, both in the analysis of sec. 2 and in the Regge/Veneziano amplitudes, isospin invari-

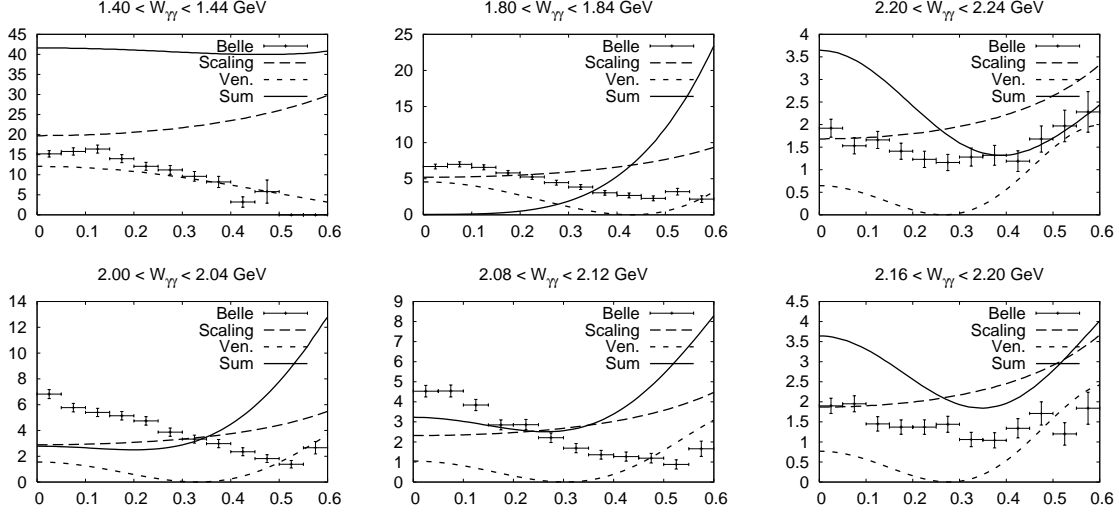


**Fig. 6.** The angular distribution of  $\gamma\gamma \rightarrow K^+K^-$  at three representative energy ranges in between 1.40 and 2.24 GeV (upper row), and between 2.00 and 2.20 GeV (lower row). We show the Belle data, the scaling contribution, the Veneziano-model contribution and the squared sum of the two. The vertical error-bars on the Belle data are statistical only.

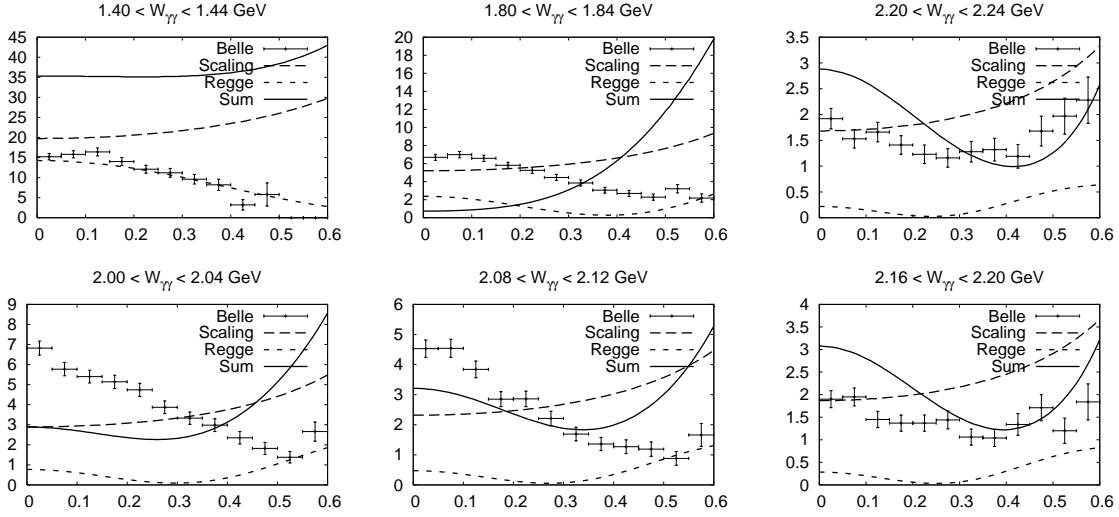


**Fig. 8.** The angular distribution of  $\gamma\gamma \rightarrow K^+K^-$ , at three representative energy ranges in between 1.40 and 2.24 GeV (upper row), and between 2.00 and 2.20 GeV (lower row). We show the Belle data against the addition of the scaling and Regge amplitudes. The vertical error-bars on the Belle data are statistical only.

ance is respected. Hence we expect:

$$\frac{\sigma(\gamma\gamma \rightarrow \pi^0\pi^0)}{\sigma(\gamma\gamma \rightarrow \pi^+\pi^-)} = \frac{1}{2}, \quad (64)$$

always, so long as the small difference in the neutral and charged pion masses can be neglected. The ratio would be violated by the inclusion of ‘cat’s ears’-type diagrams.

## 4 Conclusions

We studied exclusive hadron pair photo-production processes in low-energy photon-photon collision.

Motivated by the experimental observation of the unexpectedly large suppression of the ratio  $K_S K_S / K^+ K^-$ , we looked into the  $SU(3)$  structure of the couplings involved in these processes, adopting an  $s$ -channel picture.

We presented the calculations both for the nonet mesons and for the octet baryons. We argued that the difference between  $K_S K_S$  and  $K^+ K^-$  cross sections is due to the simultaneous presence of  $f/f'$  and  $a$  in the  $s$ -channel. The ratio is further enhanced when the  $f'$  contribution is suppressed. We argued that this could be as large as 32.

We proceeded with a model in which the ratio applies predominantly to the part of the amplitude which obeys a scaling behaviour. We added to this a long-distance am-

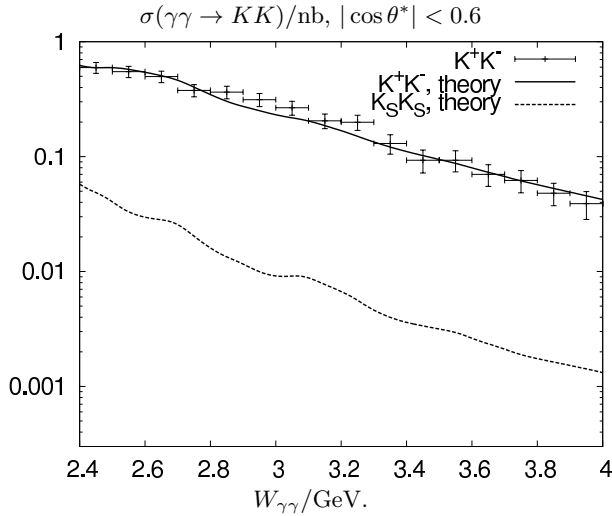


**Fig. 9.**  $\gamma\gamma \rightarrow KK$  integrated cross section in the region  $|\cos\theta^*| < 0.6$ , for  $K^+K^-$  and  $K_S K_S$ . We show the region  $2.4 \text{ GeV} < W_{\gamma\gamma} < 4 \text{ GeV}$ . We show the experimental results [2] and the sum of the scaling and Veneziano model amplitudes.

plitude whose limiting behaviour is given by Regge theory. This latter amplitude tends to be invariant under isospin.

For the  $\gamma\gamma \rightarrow p\bar{p}$  process, adopting a Regge amplitude for the long-distance dynamics, we obtain a distribution that not only fits the integrated cross section well but reproduces the behaviour of the angular distribution.

For  $\gamma\gamma \rightarrow K^+K^-$ , the long-distance dynamics was simulated using the Veneziano model. The summation of this and the scaling amplitude results in a curve for the integrated cross section that is similar to the experimental data. On the other hand, the angular distribution is not well reproduced. The Regge limiting amplitude has better fit with the data, mainly because of the reduced size of the amplitude compared to the Veneziano amplitude. In any case, the distribution near the  $f'$  peak is reproduced better by the pure Veneziano/Regge amplitudes, possibly indicating the incompleteness in our parametrization of the resonance region.

**Acknowledgements:** We thank Chen-Cheng Kuo for informative discussions on the experimental results. RCV thanks Hai-Yang Cheng for the kind invitation and support during the stay at the Institute of Physics, Academia Sinica, where part of the work was done. RCV also gratefully acknowledges the financial support by the Physics Division of NCTS. KO thanks Augustine Chen, Wan-Ting Chen and Chun-Khiang Chua for discussions.

## References

1. C.-C. Kuo et al. [Belle Collaboration], Phys. Lett. **B 621** (2005) 41 [arXiv:hep-ex/0503006];  
C.-C. Kuo, talk at Belle  $\tau/2\gamma$  meeting, Nagoya, Japan, 11–12 March 2004.

2. K. Abe et al. [Belle Collaboration], Eur. Phys. J. **C 32** (2003) 323 [arXiv:hep-ex/0309077]; H. Nakazawa et al. [Belle Collaboration], Phys. Lett. **B 615** (2005) 39 [arXiv:hep-ex/0412058];
3. V.A. Matveev, R.M. Muradian and A.N. Tavkhelidze, Lett. Nuovo Cim. **7** (1973) 719;  
S.J. Brodsky and G.R. Farrar, Phys. Rev. **D 11** (1975) 1309.
4. H. Hamasaki et al. [VENUS Collaboration], Phys. Lett. **B 407** (1997) 185.
5. M. Artuso et al. [CLEO Collaboration], Phys. Rev. **D 50** (1994) 5484.
6. P. Achard et al. [L3 Collaboration], Phys. Lett. **B 571** (2003) 11 [arXiv:hep-ex/0306017].
7. H. Aihara et al. [TPC/Two-Gamma Collaboration], Phys. Rev. Lett. **57** (1986) 404.
8. H. Albrecht et al. [ARGUS Collaboration], Z. Physik **C 48** (1990) 183.
9. W.T. Chen et al. [Belle Collaboration], arXiv:hep-ex/0609042.
10. M. Benayoun and V.L. Chernyak, Nucl. Phys. **B 329** (1990) 285; V.L. Chernyak, Phys. Lett. **B 640** (2006) 246.
11. S.J. Brodsky and G.P. Lepage, Phys. Rev. **D 24** (1981) 1808.
12. See ref. [11] and the listing under ref. 5 therein.
13. M. Diehl, P. Kroll and C. Vogt, Phys. Lett. **B 532** (2002) 99 [arXiv:hep-ph/0112274]; Eur. Phys. J. **C 26** (2003) 567 [arXiv:hep-ph/0206288].
14. See, for example, P.D.B. Collins, An introduction to Regge theory and high energy physics, Cambridge University Press, 1977.
15. A. Donnachie, H.G. Dosch, P.V. Landshoff and O. Nachtmann, Pomeron physics and QCD, Cambridge University Press, 2002.
16. A. Donnachie and P.V. Landshoff, Nucl. Phys. **B 231** (1984) 189.
17. T. Feldmann, Int. J. Mod. Phys. **A 15** (2000) 159 [arXiv:hep-ph/9907491].
18. S. Eidelman et al. [Particle Data Group], Phys. Lett. **B 592** (2004) 1.
19. M.M. Nagels et al., Nucl. Phys. **B 147** (1979) 189;  
S. Kanwar, R.C. Verma and M.P. Khanna, Prog. Theor. Phys. **62** (1979) 1152.
20. K. Igi, Phys. Rev. Lett. **9** (1962) 76;  
R. Dolen, D. Horn and C. Schmid, Phys. Rev. Lett. **19** (1967) 402;  
K. Igi and S. Matsuda, Phys. Rev. Lett. **18** (1967) 625;  
A.A. Logunov, L.D. Soloviev and A.N. Tavkhelidze, Phys. Rev. Lett. **24B** (1967) 181.
21. K. Odagiri, Nucl. Phys. **A 748** (2005) 168 [arXiv:hep-ph/0406267].
22. G. Veneziano, Nuovo Cim. **57** (1968) 190.
23. J. K. Storrow, Phys. Rept. **103** (1984) 317.
24. P. Achard et al. [L3 Collaboration], Phys. Lett. **B 536** (2002) 24 [arXiv:hep-ex/0204025].
25. S. Anderson et al. [CLEO Collaboration], Phys. Rev. **D 56** (1997) 2485 [arXiv:hep-ex/9701013].
26. C.F. Berger and W. Schweiger, Eur. Phys. J. **C 28** (2003) 249 [arXiv:hep-ph/0212066].

Total cross section

